THE ONSET OF RESONANCE-CONTROLLED INSTABILITY IN SPHERICAL BUBBLE OSCILLATIONS

R. Glynn Holt, D. Felipe Gaitan
Jet Propulsion Laboratory, California Institute of Technology
Pasadena, CA 91109

ABSTRACT

Single bubble dynamics are investigated using acoustic techniques for isolation and manipulation. The goal of the investigations is to understand the dynamic origin of the various phenomena that bubbles exhibit: light emission, enhanced mass transport, chaotic and quasiperiodic oscillations and translations. Once understood, acoustically manipulated bubbles can serve as platforms for materials effects on free surfaces, using surfactants to alter surface rheology and observing how that affects both dynamics and also mass transport. The effects of gravity on the problem will be shown to be significant. The first set of observations from 1g experimentation are presented. These observations are of the onset conditions for instability of the spherical shape of the bubble. For the size range 55 - 90 microns in diameter we observe instability governed by resonant mode coupling, which is significantly affected by the buoyant force and its effects.

INTRODUCTION

A bubble is a laboratory for the study of a surprising variety of physics problems. Heat transport [1], mass transport [2], surfactant effects [3], shock waves [4], chaos [5], free surface instability [6], and even electromagnetic radiation [7] are all phenomena associated with the highly nonlinear oscillations of air bubbles in water. It is impossible, however, to separate the study of any of these phenomena from the fundamental mechanics of the bubble wall's oscillation, coupled to the thermodynamics of the interior. Thus it is crucial to make detailed observations of bubble mechanics in concert with other investigations of material or transport properties.

Many areas of science and technology depend on bubble dynamics. In the field of biomedical ultrasound, many of the effects studied in the ultrasound community (such as enhanced cell lysis, sonochemical reactions, ultrasonic cleaning, etc.) depend on the mechanical response of a bubble to a sound field. In the field of surface rheology, knowing the mechanical response of bubbles lets us use them as tools to probe the effects of surface active agents, much as drops are currently being used [8]. In addition to being a closed, isolated interface, one of the major reasons a bubble is used in these contexts is that a bubble can produce both pure dilatational, shear, and a combination of dilatational and shear interfacial motions. Mass transport research on the effect of surfactants on the diffusion of gas across the air water interface [Fyrillas and Szeri in 3] also relies on detailed bubble mechanics, and will eventually lead to understanding the fundamentals of air-sea mass transfer. Ambient noise in the ocean (which has been shown to be largely due to volume oscillations of bubbles near the sea surface [9]) has been conjectured to depend on precisely the nonlinear shape/volume mode energy transfer for which we present results in this paper [10].

In the microgravity environment, bubbles are important for two reasons. The first is that bubbles experience a buoyant force due to gravity, and the justification for microgravity experimentation is simply the removal of the buoyant force and its effects. Static deformation of the equilibrium shape changes the *very nature* of the coupling between volume and shape mode(s) , which we will show is the primary instability for a bubble [11]. As well, translatory oscillations of the bubble guarantee that the onset of shape oscillations in **1g** will occur at relatively low pressure values, making *impossible* the observation of the predicted volume-oscillation bifurcation superstructure [12].

Bubbles are best studied in isolation, without contact and contamination from containers, and then non-invasively manipulated. Perhaps the most effective scheme is that of acoustic levitation, where the nonlinear acoustic radiation force balances the buoyant force in 1g, and merely positions at

pressure maximum in **0g**. On the practical side, however, measurements on bubbles in **1g** are compromised because positioning is coupled to driving force, and nonlinear effects such as self-oscillation and streaming occur due to the coupling (via the necessarily high-amplitude acoustic field) of the volume and translational modes. Decoupling driving from positioning is *impossible* in **1g**.

Secondly, apart from bubbles being the subjects of microgravity research themselves, *bubbles occur in fluids in space*, and their appearance is fraught with problems, not least of which is how to get rid of them! Fluids experiments (Drop Physics Module, Zeolite Crystal Growth, Oscillatory Thermocapillary Flow, Generic Bioprocessing Apparatus) on both the STS-50 and STS-73 missions have often developed bubbles whose presence and dynamics affected what was being measured. Most proposed schemes for elimination of unwanted bubbles (acoustic, thermocapillary, electrophoretic) depend on dynamics of bubbles for their efficacy. Once again understanding bubble mechanics is seen as fundamental to a host of practical problems.

We present here the results from the first phase of our planned experimentation: the investigation of the onset of non-spherical oscillations of the shape of the bubble. These Faraday shape oscillations form a natural boundary in the parameter space of bubble dynamics, since experimentation on spherical bubbles can occur only at pressures and radii below the critical values. Above the threshold, the amplitude of these shape oscillations can rapidly grow, and lead to breakup of the bubble. We will limit ourselves to a brief descriptive background of the problem, followed by an experiment description and results.

BACKGROUND: THE SHAPE OSCILLATION PROBLEM

A gas/vapor bubble in water is a highly nonlinear system. This is most readily seen when the bubble is subject to an external forcing, such as is the case when a time-varying acoustic field is imposed. Suppose that the acoustic wavelength is much larger than the bubble radius R_0 ($k_a R_0$ small, where k_a is the acoustic wavenumber in water). During a compression phase of the field, the bubble, since it is highly compressible, will contract, accelerating inward. The pressure and temperature will increase. Eventually, the contraction halts, reverses, and the bubble begins expanding. During the expansion phase of the external field, the bubble expands, cooling and reducing the pressure in its interior.

This oversimplified picture gives us at least a qualitative insight into the motion. The nonlinear restoring force is largely thermodynamic during collapse (due to the increased interior pressure) and expansion, since equilibrium implies a static pressure stress balance across the bubble wall. The nonlinear damping is due to thermal, bulk viscous and sound radiation mechanisms in the case of a pure liquid, and additionally due to surface viscosity for liquids with surfactants. For a fixed equilibrium radius R_0, the bubble will exhibit a fundamental linear resonance frequency f_0. For an air bubble in water of radius $R_0 = 64$ microns, $f_0 \sim 50$ kHz at atmospheric pressure.

Consideration of the spherically symmetric problem yields predictions of highly nonlinear dynamics as the acoustic pressure P_a is increased. Numerical integration of the equation of motion for a driven, *spherical* bubble predicts the resonant creation of *periodic* (and via standard period-doubling bifurcations *chaotic*) families of solutions via resonant *saddle-node* bifurcations. The Farey ordering [12] of the resonant saddle-node bifurcations imposes a recurrent superstructure which controls the appearance of period-doubling bifurcations to chaos. One of the goals of this research is to observe this behavior, or determine why it is not observed.

Under what conditions will spherical symmetry become unstable, and further under what conditions will this instability lead to observable distortions of the shape and eventual breakup of the bubble? There are two candidate instabilities: Rayleigh-Taylor (RT, [13]), and parametric or Faraday (F, [14]). It can be shown that, during at least some part of its motion, a bubble is RT unstable. RT instability occurs for accelerated interfaces when density and pressure gradients across the interface are opposed. RT occurs on a fast time scale, and is thus likely to be violent in its effects on the bubble surface if conditions allow it to develop. At first glance, RT appears very likely to destroy a bubble at its first collapse.

F, in contrast, requires a *resonant interaction* for the necessary energy exchange. A free liquid surface, when vibrated periodically and normal to its surface plane, will exhibit Faraday waves with *half* the driving frequency when the excitation overcomes the damping [15]. In addition to requiring a finite threshold excitation, sufficient time is required for the coupling to occur, typically 2 or more cycles of the periodic excitation. Finally, since a bubble is a closed surface whose circumference is of the same order as the capillary wavelength, the energy must excite a normal mode of the bubble, constrained by a resonance condition similar to the classic $f_{shape} / f_{volume} = 1/2$, and consideration must be given to the damping of the normal modes. Theoretical treatments of this problem [Strube, Eller and Crum in 6] predict that such instabilities will occur near the $(P_a R_0)$ values where the interesting spherical dynamics occurs. Thus, we want to resolve the issue of the dynamical behavior of bubbles over a wide range of parameter space $(P_a R_0)$: what behaviors obtain, and why?
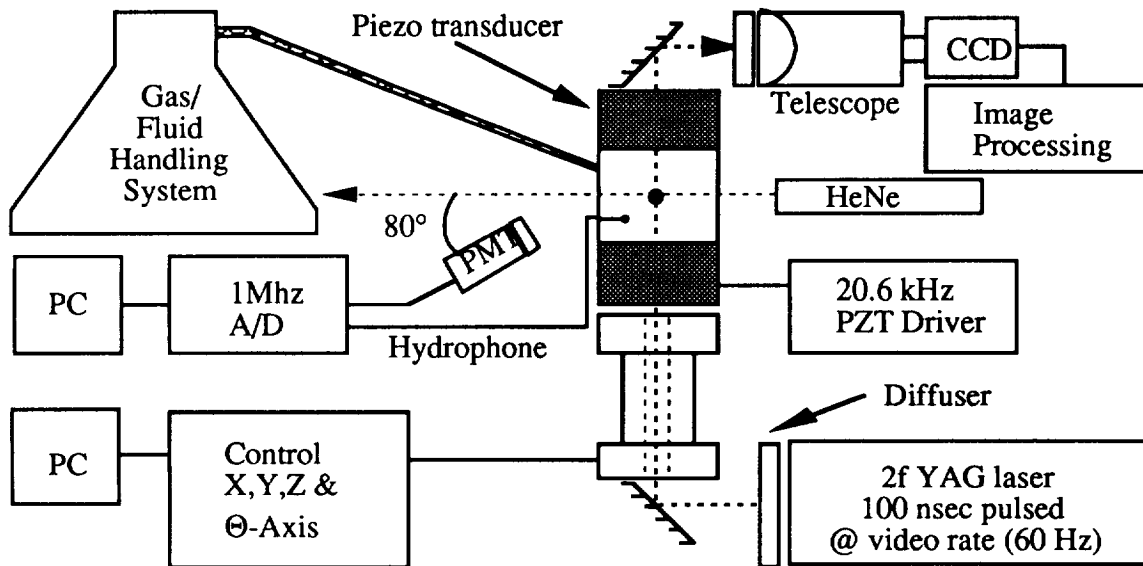
EXPERIMENT

Figure 1: Schematic of setup for acoustically levitating and imaging bubbles in water

Air bubbles initiated via electrolysis are acoustically levitated in water in the $f_a = 20.6$ kHz standing wave field of a cylindrical resonance cell as illustrated in Fig. 1 [16]. The acoustic pressure P_a at the antinode is obtained from a custom hydrophone mounted near the z antinode and 1cm away from the side wall inside the cell. The hydrophone is calibrated by balancing the buoyant force with the acoustic force for a variety of bubble sizes and positions along the z axis pressure gradient, always using small amplitude oscillations. For calibration purposes, R_{ave} $(= R_0$ for a linearly oscillating bubble) is measured directly by measuring the locations of the peaks encountered by sweeping a detector from 20° to 90° in the polarization-plane forward scattering of an incident linearly polarized He-Ne beam using Mie theory [17]. R_0, R_{max} and R_{min} are obtained from single frame video images illuminated at 1 pulse per frame (maximum 1 ms pulse width); R_0 in particular is obtained by turning the sound field off instantaneously when the bubble is in the focal plane of the imaging system. $R(t)$ is obtained from a PMT located at 80° from the forward [18]. Corroborating $R(t)$ information is obtained from a fast photodiode directly in the forward diffraction lobe of the bubble. Distilled, de-ionized, carbon and particulate filtered water was used for all measurements. Dissolved gas concentrations less than saturation were obtained by allowing the water to equilibrate at a reduced pressure.

The practical key to performing the measurements we report here is the slowing of the mass transport time scale within two pressure constraints: our lowest obtainable pressures are bounded by the minimum trapping pressure, while the highest obtainable pressures (for a given R_0) are bounded by the threshold for Faraday shape oscillations and breakup of the bubble. Within these bounds, for a fixed P_a and dissolved gas concentration, the system will self-select one (or very few) bubble size R^* which will be in dynamic mass equilibrium. By varying the dissolved gas concentration we can cause that size range to span the entire space from 1 to 100 microns. We can vary P_a near R^* where dR_0 / dt is small, and observe the onset of shape oscillations quasistatically.

RESULTS

At low P_a, the bubble remains spherical, and exhibits the weak nonlinear trait of harmonic generation [16], with the response remaining periodic with the same period T_a as the acoustic field. Figure 2a shows the measured P_a and R as functions of time; note the strong 2nd harmonic component. The bubble in Figure 2 had an equilibrium size of 66 microns, and a linear resonance frequency of 48 kHz, very nearly twice the acoustic frequency f_a. The pattern repeats itself for smaller bubbles as their linear resonance frequency nears an integer multiple of f_a. Thus, we observe the pre-saddle-node harmonic resonance predicted by theory. However, all the spherically symmetric oscillations we have observed have been strictly periodic with period T_a, and remain below the amplitudes required for the saddle-node bifurcation predicted. What prevents this bifurcation?
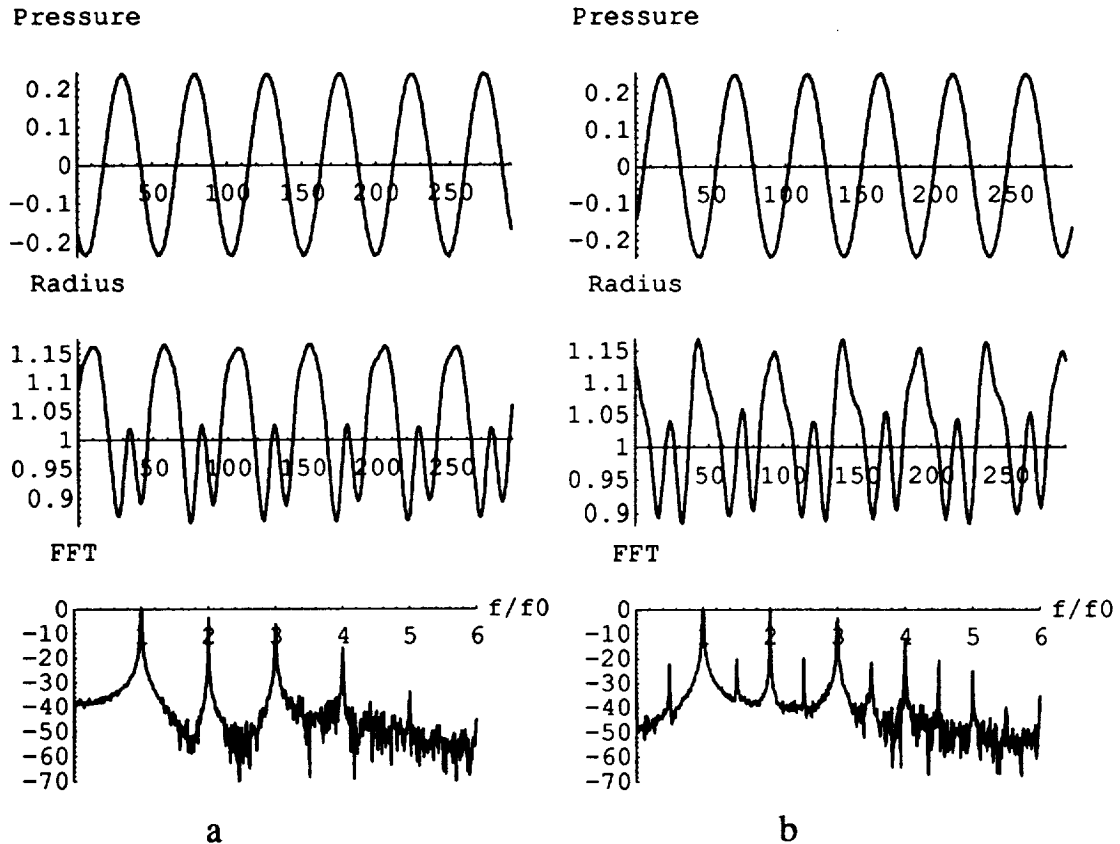

Figure 2: Response of a 66 micron radius bubble to an acoustic pressure of 0.24 bar at 20.6 kHz. a) from top to bottom: the pressure vs time (arbitrary units) from the hydrophone; normalized radius vs time from the 80° PMT scattered light; and FFT of the radius. b) The same data at 0.25 bar, just after the onset of a mode 5 shape oscillation. The signature of the shape oscillation is the peak at f/f0 = 1/2.

Our observations show that, for all acoustic pressures P_a below 1.3 bar for air bubbles in water, the instability which develops first is the Faraday instability. The signature of this instability is often a period-doubling of the scattered laser signal, as shown in Fig. 2b for a 66 micron bubble driven just past the onset of the 5-lobed mode, identified by video image analysis. Figure 3 shows a subset of the measured $(P_a R_0)$ values for onset of an oscillation of the shape of the bubble, and thus the loss of spherical stability. The observed modes are indicated by the symbol type. Notice also the set of theoretical curves for onset of the different modal oscillations: we will discuss these in the next section. We concentrate on understanding the experimental data in simple terms in this section.
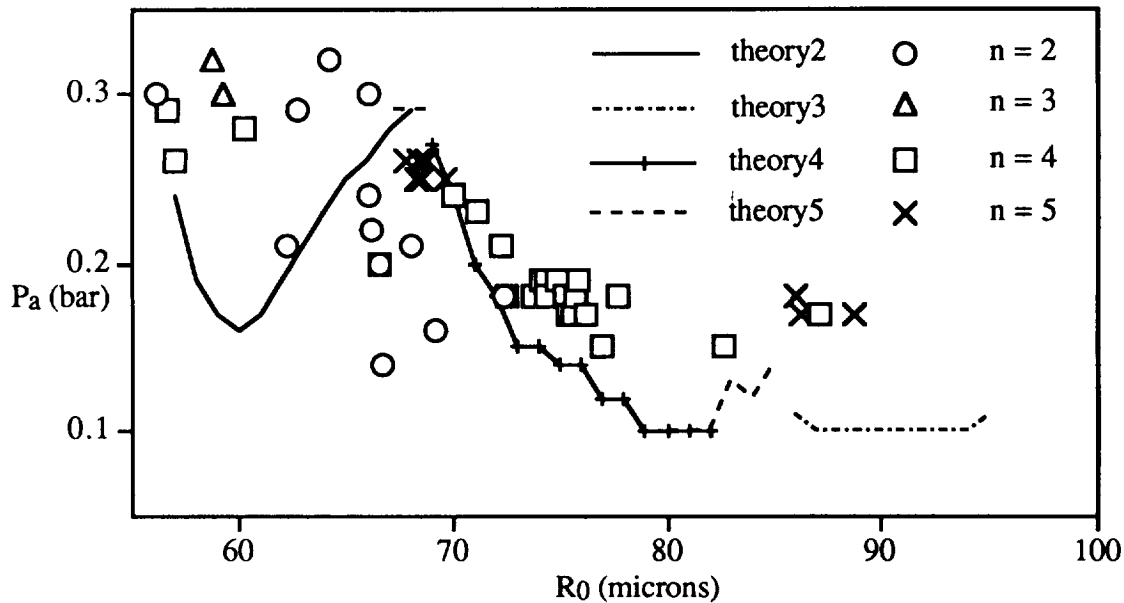

Figure 3: Measured threshold acoustic pressure Pa and equilibrium radius R0 for onset of shape oscillations (Faraday instability: mode observed given by symbol). All data presented are for air bubbles levitated in pure water driven at 20.6 kHz at 22° C at ambient pressure of 1 bar. The theoretical thresholds and modes presented for comparison are courtesy of M. Brenner, calculated using the algorithm presented in [6].

The general trend of higher threshold at smaller bubble size (averaged over different modes) is just the stabilizing effect of the curvature $1/R$. Most of the dips and peaks, and the presence and location of specific normal modes can be understood in terms of resonances. A particular shape mode n is in *external resonance* to the driving field (via the forced non-resonant response of the volume mode) when $f_n / f_a \sim i / 2$, $i = 1,2,3,...$, and we speak of i:2 external resonance. A shape mode n is in *internal resonance* with the resonating volume mode when $f_n / f_0 \sim j / 2$, $j = 1,2,3,...$, hence j:2 internal resonance . Understanding that the energy transfer mechanism is the Faraday instability is the reason for the factor of 2 in the denominator. The locations in (P_a, R_0) space where i and j are integers are not in general coincident. For bubbles in the range presented here, either resonance is equally likely; for very small bubbles, only internal resonance is possible at kHz frequencies. Note that, though we use the classification 'shape modes in external resonance with the driving field', the field does not directly force the modal oscillation.

Figure 4 plots the ratio of mode (shape or volume) frequency to acoustic driving frequency fa using the measured R_0 and the observed mode number (assumed axisymmetric) at the onset of shape oscillation. Analytical curves for the Lamb frequency [19] for the shape modes 2 - 5 are plotted, as is an analytical expression for the fundamental linear resonance frequency for the volume mode [20] at ambient pressure. Thus, points where the halved volume frequency curve intersects any shape modal frequency curve (e.g., the $n = 4$ curve near 60 microns) represent the condition for 1:2 internal resonance, or $j = 1$ [a slightly different definition from that of Feng et al. in 21]. Points where a shape frequency curve intersects a line $i = 1, 2, 3$ represent i:2 external resonance: e.g., $i = 1$ for the $n = 2$ curve near 60 microns.
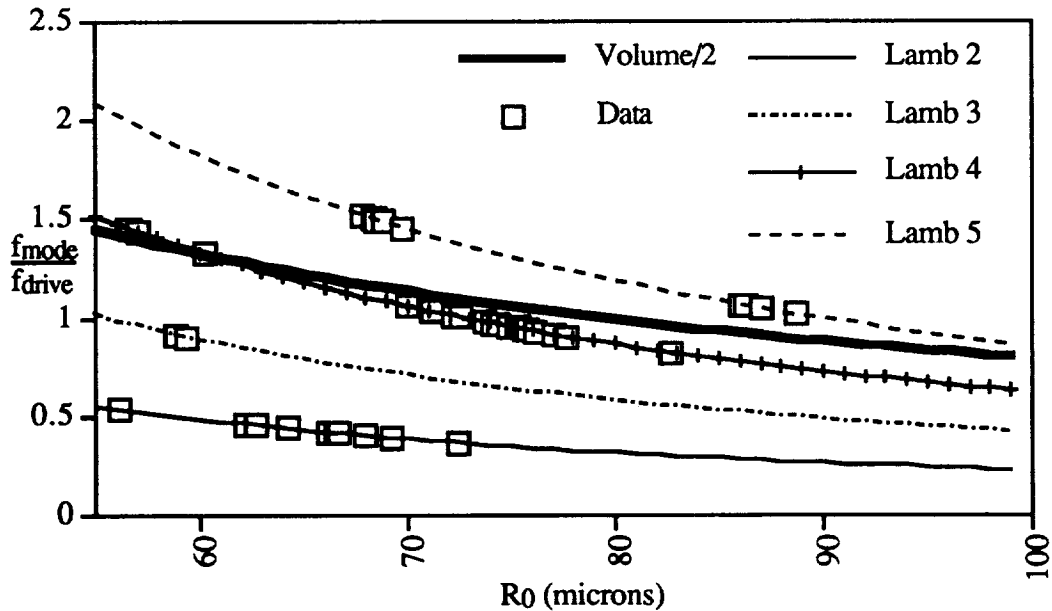
2.5

2

$\frac{f_{mode}}{f_{drive}}$ 1.5

1

0.5

0

Volume/2 — Lamb 2
□ Data ·········· Lamb 3
—+— Lamb 4
----- Lamb 5

R_0 (microns)

60 70 80 90 100

Figure 4: Shape and volume modal frequencies vs R_0. The points labeled Data are the theoretical shape frequencies calculated for the observed mode and R_0. Curves labeled 'Lamb n' were generated using the analytical expression of Lamb [19] for capillary waves. The curve 'Volume/2' is the analytical approximation to the linear resonance frequency of the volume mode due to Minneart [20].

Figure 4 clearly shows the organizing principle of resonance: the data fall in bunches near points of internal or external resonance. The origin of the peak and valley in the measured threshold between 60 and 70 microns is clear: it is due to an approximate 2:1 external resonance of the $n = 2$ mode. The observation of the $n = 4$ mode at onset between 70 and 80 microns is due to a *double resonance*: $j \sim 1$ and $i \sim 2$ simultaneously (this region is usually called the '2nd harmonic' resonance, since the bubble's linear volume frequency is twice the driving frequency, and the bubble oscillates nonlinearly with a strong $2f_a$ component near this size).

DEVIATIONS FROM THEORY: THE EFFECT OF GRAVITY

The theoretical threshold curves in Figure 3 were generated using a technique presented in Brenner et al. [6]. The radius variable in the nonlinear 2nd order ODE describing spherical bubble dynamics [the 'Rayleigh-Plesset equation', 22] is replaced by an expansion in normal shape modes described by Legendre polynomials. A linear-form 2nd order ODE for the amplitudes a_n of the shape modes n is derived, possessing nonlinearly time-varying coefficients (a generalization of Hill's equation). This approach can account for both internal and external resonances of all orders, but does not account for the effect of the buoyant force.

In Fig. 3 we see good agreement for the location of the threshold for the 4 mode, and fair agreement for the 5 mode. The 3 mode appears to be in disagreement, but this is partially due to the fact that it becomes more important in the ranges 15 - 40 microns, and for 90-110 microns; we see the 3 mode often in these regimes, but the data is not yet fully reduced.

The effect of gravity can be seen in the striking disagreement between theory and experiment for the 2 mode between 60 and 70 microns in Figure 3. Experiment shows the 2 appears initially at larger pressures than the theory predicts, and then a strong resonance dip to onset at anomalously low pressures occurs. Figure 4 reveals that these data are all in 1:2 external resonance with the acoustic field via the nonresonant (entrained) response of the spherical volume pulsations. How can the presence of gravity explain this?

The key is the slight deformation of the bubble due to the balance of the time-averaged acoustic force and the buoyant force. Marston [23] showed theoretically that the primary spatial component of the acoustic force was the quadrupole ($n = 2$) term. Holt et al. [24] among others have

verified this for larger bubbles. Yang, Feng and Leal [21] investigated the influence of an external pressure or flow field with quadrupole spatial characteristics on the resonant coupling. In particular, they found that not only were energy-exchange and stability different from the free-field cases previously studied, a different coupling mechanism was discovered, of $O(3/2)$. One general conclusion was that mode-mode coupling was significantly enhanced over the free-field case, and more likely to occur at lower amplitudes (and hence lower driving pressures).

Thus, the resonance dip between 65 and 70 microns is explained: the quadrupole deformation due to the buoyant force lowers the necessary threshold for onset of shape oscillations. Things are not as clear in attempting to explain the appearance of the 4 mode near 60 microns, but enhancement of the 2 - 4 mode coupling is possible, since the theory predicts the 2 should be excited. However, at 60 microns the 4 mode is in 1:2 resonance with the volume mode, providing an alternative explanation.

CONCLUSION

Understanding the nonlinear dynamics of driven bubble oscillations is important as a basic problem in fluid physics and nonlinear dynamics. There exists a complex set of behavior(s) whose observation depends on nonlinear resonant coupling, internal resonances and their structures, initial conditions and external parameters and fields. The implications this understanding will have for other fields in which bubble phenomena play a role will be far-reaching. The research presented here represents a first step towards a global understanding of bubble behavior. The future directions of this reserch as outlined above all depend on an accurate and quantitative understanding of the nonlinear mechanics of bubble oscillations. Gravity has significant and subtle effects effects on the problem, and it is clear that *microgravity* experimentation would provide both qualitative and quantitative improvements. The dominance of surface tension forces and the lack of a buoyant force would not only enable direct comparison with theories, but would allow access to parameter space forbidden in **1g** due to the need for levitation.

REFERENCES

1. Yasui, K., J. Acoust. Soc. Am. **98**, 2772 (1995).
2. Löfstedt, R. et al., Phys. Rev. E **51**, 4400 (1995).
3. Crum, L.A., J. Acoust. Soc. Am. **68**, 203 (1980); Johnson, D.O. and K.J. Stebe, J. Colloid Interface Sci. **168**, 21 (1994); Fyrillas, M.M. and A.J. Szeri, J. Fluid. Mech. **289**, 295 (1995).
4. Hickling, R. and M.S. Plesset, Phys. Fluids **7**, 7 (1964); Wu, C.C. and P.H. Roberts, Phys. Rev. Lett. **70**, 3424 (1993).
5. Holt, R.G., D.F. Gaitan, A.A. Atchley and J. Holzfuss, Phys. Rev. Lett. **72**, 1376 (1994).
6. Birkhoff, G., Q. Appl. Mech. **12**, 306 (1954); **13**, 451 (1956); Strube, H.W., Acustica **25**, 289 (1971); Hullin, C., Acustica **37**, 64 (1977); Brenner, M.P. et al., Phys. Rev. Lett. **75**, 954 (1995).
7. Marinesco, N. and J.J. Trillat, Proc. R. Acad. Sci. **196**, 858 (1933); Gaitan, D.F. et al., J. Acoust. Soc. Am. **91**, 3166 (1992); Barber, B.P. and S.J. Putterman, Nature **352**, 318 (1991).
8. Tian, Y., R.G. Holt and R.E. Apfel, Phys. Fluids **7**, 2938 (1995).
9. Prosperetti, A., H.C. Pumphrey and L.A. Crum, J. Geophys. Res. **94**, 3255 (1989).
10. Longuet-Higgins, M.S., J. Fluid Mech. **201**, 525 (1989a); 543 (1989b); **224**, 531 (1991).
11. Holt, R.G. and D.F. Gaitan, APS Bulletin **40**, 1960 (1995).
12. Parlitz, U., V. Englisch, C. Scheffczyk, and W. Lauterborn, J. Acoust. Soc. Am. **88**, 1061 (1990).
13. Taylor, G.I., Proc. Royal Soc. A **201**, 192 (1950).
14. Faraday, M. Phil. Trans. Royal Soc. London **121**, 299 (1831).
15. Miles, J., J. Fluid Mech. **248**, 671 (1993).
16. Holt, R. Glynn and Lawrence A. Crum, J. Acoust. Soc. Am. **91**, 1924 (1992).
17. Lentz, W.J. et al., Appl. Opt. 34, 2648 (1995).
18. Holt, R. G. and L. A. Crum, Appl. Opt. **29**, 4182 (1990).
19. Lamb, H., *Hydrodynamics* (Dover, New York, 1945).
20. Minnaert, M. Phil. Mag. **16**, 235 (1933).
21. Mei, C.C. and X. Zhou, J. Fluid Mech. **229**, 29 (1992); Feng, Z.C. and L.G. Leal, Phys. Fluids **5A**, 826 (1993); Yang, S.M., Feng, Z.C. and L.G. Leal, J. Fluid Mech. **247**, 417 (1993).
22. Rayleigh, Phil. Mag. **34**, 94 (1917); Plesset, M.S., J. Appl. Mech. **16**, 277 (1949).
23. Marston, P.L., J. Acoust. Soc. Am. **67**, 15 (1980).
24. Holt, R.G. and E.H. Trinh, J. Acoust. Soc. Am. **95**, 2938 (1994).